ADVANCED FUNCTIONAL MATERIALS
www.afm-journal.de

Agarose Micro/Nanostructured Surfaces: A Step Toward an Innovative Solution for Platelet Storage Bags

*Gurunath Apte, Marcus Soter, Dikshita Madkatte, Doris Heinrich, and Thi-Huong Nguyen**

In addressing the critical limitations associated with platelet storage, the study investigates an innovative solution aimed at preventing the unwanted activation of platelets within storage bags. This activation is a key factor that currently restricts the shelf life of platelet products to only 72 h, leading to extreme waste production and high costs. Here, highly effective surfaces are identified for minimizing surface-induced platelet activation. Using thermal nanoimprint lithography (T-NIL), a new method is demonstrated for patterning reproducible agarose micro/nanostructures (a natural hydrogel with anti-platelet adhesive properties) including dots, chains, pills, and squares. The agarose (3%) structured surfaces displayed outstanding flexibility and hydrophilic behavior that prevented platelet adhesion as confirmed by confocal microscopy. Importantly, pill-shaped structures effectively maintained their ability to prevent platelet adhesion, even after a long cell-contacting duration. Atomic force microscopy indicated that the effectiveness of dampening platelet adherence is determined by the shape, size, height, and aspect ratio of the structures. A model is provided to explain how the different shapes affect wettability and thereby hinder platelet adherence. The developed anti-adhesive agarose structured surfaces show promise to revolutionize platelet storage, provide vital insights into biomaterials research, and demonstrate the potential of tailored agarose surfaces in biomedical applications.

1. Introduction

Platelets are indispensable in medical interventions, particularly in transfusion medicine, where they play a crucial role in managing bleeding disorders and supporting patients undergoing surgeries or chemotherapy. The global demand for platelet concentrates is substantial, with ≈1300 liters being transfused daily in Germany alone,[1] and over 118 million blood donations collected worldwide annually.[2] The significance of accessible platelet concentrate for trauma patients has been highlighted as a matter of life and death.[3] However, a significant challenge arises in the realm of platelet storage management, particularly for smaller hospitals that often struggle to stock platelets.[3] Even in larger centers, platelet concentrates are primarily allocated to hematology-oncology patients only, creating an imbalance in distribution.

Current technologies allow the storage of platelets at room temperature for only 4 days in Japan, 5 days worldwide, and 7 days in the US (only in some special blood services if they meet several FDA requirements).[4,5] The short shelf life together with unpredictable demand results in platelet inventory management problems as manifested by high rates of outdating, frequently reported at 10% to 20%.[6] The World Health Organization's recommendation of a mere 72-h shelf life after collection[5] further contributes to elevated wastage and increased costs in the blood supply chain. The short storage period limits platelet transfusion in many emergency stations. As a consequence, platelet transfusions are only recommended for patients with life-threatening bleeding to preserve the limited platelet inventory, and platelet transfusion thresholds will be lowered during critical times of blood product shortage.[7]

The main problems leading to the short shelf life of platelet products are platelet dysfunction and bacterial contamination.[8–12] Unlike red blood cells, the dynamic nature of platelets makes them highly sensitive to storage conditions and easily activated. Stimulated platelets release bioactive substances,[13,14] collectively known as the "platelet storage lesion," including altered metabolism, reduced response to agonists, and an increased risk of bacterial contamination, a major problem during platelet storage.[8,15] A similar or even more complicated thrombogenic mechanism can occur on many medical devices such as transfusion apparatus and implants.[16] Treatment with expired or low-quality platelets decreases transfusion efficacy and increases adverse events

G. Apte, M. Soter, D. Madkatte, D. Heinrich, T.-H. Nguyen
Institute for Bioprocessing and Analytical Measurement Techniques (iba)
37308 Heilbad Heiligenstadt, Germany
E-mail: thi-huong.nguyen@iba-heiligenstadt.de
M. Soter, D. Madkatte
Karlsruhe Institute of Technology
76131 Karlsruhe, Germany
D. Heinrich, T.-H. Nguyen
Faculty of Mathematics and Natural Sciences
Technische Universität Ilmenau
98694 Ilmenau, Germany

The ORCID identification number(s) for the author(s) of this article can be found under https://doi.org/10.1002/adfm.202414096

DOI: 10.1002/adfm.202414096

such as sepsis and immune-mediated events, especially, in hematology, oncology, and post-cardiac surgery patients.[9] The short shelf life of platelet storage poses a significant challenge in the field of transfusion medicine and blood banking. Thus, maintaining platelet integrity requires continuous supply and precise inventory management. Despite decades of efforts, improving blood-contacting materials still remains exciting. Addressing platelet storage issues is vital for enhancing transfusion outcomes and ensuring a stable blood supply chain.[17]

To date, improvement of platelet storage bags mainly targets challenges like the short shelf life and platelet storage lesions. Innovations encompass improvements in additive solutions, pathogen reduction, temperature control, bioreactor systems, monitoring, smart packaging, sensors, and materials for containers. Material selection is crucial as biocompatibility, flexibility, gas permeability, and preventing platelet activation should be considered. To date, various materials, including polyolefins, ethylene vinyl acetate, polyurethane, fluoropolymers, blends, silicone, di-2-ethylhexyl phthalate, and polyethylene terephthalate, have been explored but exhibited several limitations.[18,19] For example, despite concerns about toxic plasticizers like di-2-ethylhexylphthalate,[20–23] this material has still been in use since the mid-20th century.[24,25] To date, addressing bag surface-induced platelet activation remains an understudied challenge.

To improve bag materials, chemical modifications are often considered[26] but face long processes involving many regulatory challenges to commercialize the product. Superhydrophobic and zwitterionic polymers are well-known approaches for surface modification to enhance hemocompatibility in blood-contacting medical devices.[27,28] Wu et al. reported potential contributions of superhydrophobic surfaces to avoid fouling.[29] Characterized by lower surface energy, these surfaces offer promising self-cleaning potential that contributes to antifouling effects.[29] Meanwhile, numerous studies have demonstrated the effectiveness of zwitterionic polymers. Xiang et al. reported that zwitterionic membranes exhibit significant resistance to protein and platelet adhesion while maintaining exceptional antithrombogenicity due to their excellent wettability characteristics.[30] Despite these advancements, antifouling coatings for blood-contacting devices still face numerous challenges and unresolved issues that require further investigation.[28] In recent developments, there has been a focus on topographical modifications using already approved materials for engineering novel structured surfaces.[31–38] While various antifouling materials can prevent platelet-surface adhesion, micro- and nanostructures further improve characteristics such as wettability and mechanical properties compared to their flat surfaces. The cavities of the structured surfaces can embed platelets leading to a reduction of platelet spreading and activation.[34] Koh et al demonstrated that submicron features led to a significant decrease in platelet adhesion, however, larger features of structures did not exhibit the same effect.[32] Under shear conditions, bioinspired microstructured surfaces prevented platelet adhesion by up to 78%.[39] Together, these findings underscore the importance of structured surfaces at submicron to minimize platelet-surface interactions. This approach not only ensures compliance with established standards but also minimizes efforts for the commercialization of products. Recently, others and our group proved that micro/nanostructures prevent platelet adhesion/activation due to their ability to influence cellular behavior at a fundamental level, making them promising candidates for the development of storage bags.[31–38,40] Different materials for fabricating structures have been investigated, including polymers such as polydimethylsiloxane and polyurethane, biodegradable polymers like polylactic acid, hydrogels including polyethylene glycol and alginate, metals like titanium and gold, silicon-based materials, biomimetic coatings, composite materials, nanostructured coatings, bioceramics like hydroxyapatite, and carbon nanotubes.[31–38] Various methods have been employed for the fabrication of micro/nanostructures such as electron beam lithography, nanoimprint lithography, soft lithography, atomic layer deposition, chemical vapor deposition, self-assembly, and focused ion beam, each offering specific advantages but also grappling with substantial challenges.[41] These include resolution limitations, intricacies in operation, slow processing speeds, throughput issues, the requirement for costly equipment, concerns about replication quality, non-uniform film thickness, the need for precision in structure creation, potential damage to sensitive materials during the process, and constraints in material selectivity. Despite many efforts, the best material for imprinting micro/nanostructures, especially for platelet applications, has not yet been identified.

Agarose is a polysaccharide derived from red algae and stands out as a promising "green" material due to its biocompatibility, biodegradability, gel-forming ability, and adaptability to mimic biological environments.[42,43] It is primarily utilized in various applications such as molecular biology, biochemistry, and medical research.[44,45] Despite these advantages, agarose has not been extensively explored for the development of platelet-contacting devices. We have recently found that the inert, easily fabricated, and stable agarose flat film has a great capacity to prevent platelet adhesion and activation.[46] Furthermore, iron oxide nanoparticles that exhibit antimicrobial characteristics could be effectively incorporated into the gels without causing platelet activation.[46] Even though micro/nano topographies prevent platelet adhesion/activation on several materials,[31–38] the effect of agarose structured surfaces on platelets has not yet been explored.

In this study, we employed agarose as a "green" resist for engineering micro/nanostructures utilizing thermal nanoimprint lithography (T-NIL), a high-resolution, cost-effective, and versatile technique with high throughput, reproducibility, and scalability.[47] We fabricated agarose surface structures of different shapes including dots, chains, pills, and squares to pinpoint the most effective features that exhibit strong anti-platelet adhesion properties. A comprehensive characterization of agarose films and structured surfaces, investigating parameters such as sizes, diameters, feature heights, aspect ratios, and surface contact angles was conducted. To evaluate the platelet response on agarose structures, platelets were allowed to interact with materials, and the number and size of adhered platelets on each distinct structured surface were meticulously quantified at different time points. Identification of suitable "green" agarose structured surfaces can be a potential breakthrough in platelet storage technology and other medical applications.

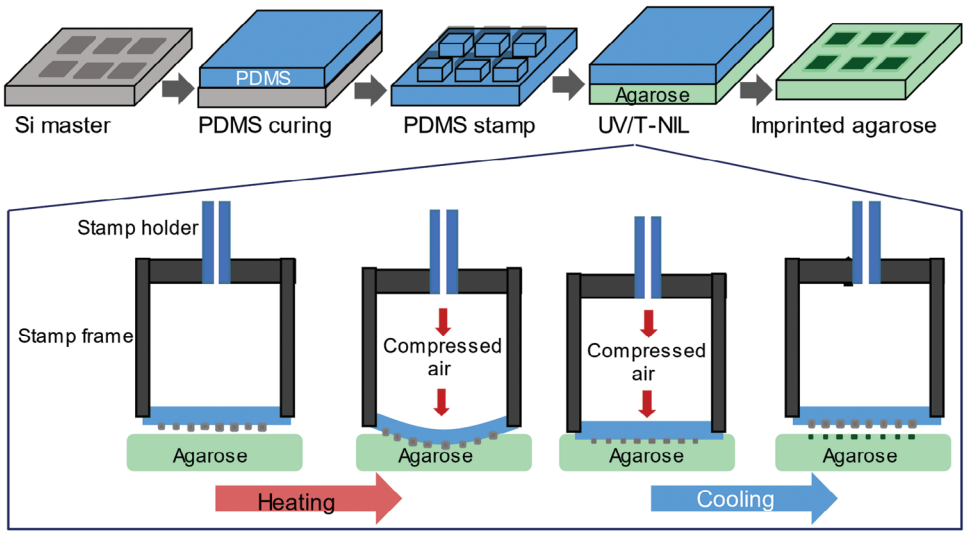

Figure 1. Schematic representation of the imprintation process for micro-/nanostructured arrays in agarose using T-NIL. (Top) Illustrations depict the fabrication process of the PDMS stamp before the creation of imprinted agarose structures. (Bottom) Detailed T-NIL imprinting process, highlights in particular the deformation of the flexible PDMS mold when compressed air is introduced to contribute to the formation of precise micro-/nanostructured patterns on the agarose surface.

2. Results

We investigate the hypothesis that the geometrically structured agarose film plays a pivotal role in influencing platelet adhesion. For that, the mechanical properties of the agarose base were first investigated. Subsequently, optimal printing parameters for T-NIL were meticulously established to ensure the fabrication of stable and reproducible structures. Various structural motifs such as dots, chains, pills, and squares were then fabricated and characterized. Freshly isolated platelets were subsequently incubated on these surfaces at various time points to assess platelet adhesion capacity. The number of bound platelets on each surface was quantified to facilitate a comparative analysis of the effects among different structured surfaces.

2.1. Fabrication of Micro-/Nano Agarose Structures

In the process of generating agarose micro-/nanostructured arrays via T-NIL, the initial step is the fabrication of polydimethylsiloxane (PDMS) stamps. These stamps were produced by molding the structures from the pre-structured silicon master using PDMS. Following the curing of the PDMS, the resultant stamps were then carefully applied to the resist, initiating the formation of micro-/nanostructured arrays through T-NIL (**Figure 1**, top). Resists are crucial components in the T-NIL as they act as a guide for transferring patterned features from the mold onto the substrate. In T-NIL, the mold is pressed against the heated resist to form the pattern and then removed to reveal the patterned substrate.[47] To delve into the intricacies of the T-NIL process for imprinting structures, a detailed depiction is provided (Figure 1, bottom). During this process, the PDMS stamp, securely mounted in a frame holder, leads to compression of agarose film under heating conditions. Subsequently, upon cooling, the stamp was removed from the agarose, leaving behind the intricately imprinted structures on the agarose surfaces.

To ensure the fabrication of stable and reproducible structures, not only the agarose concentration but also several printing parameters including heating temperature, float delay time (the time for the molten agarose to achieve a complete filling of all cavities), and compressed air pressures requires optimization. Here, the heating time was selected (180 s) so that the agarose film takes on the desired temperature homogeneously. Furthermore, the cooling time was selected (240 s) so that the agarose film reaches room temperature even after heating to 90 °C. The pre-pressure of the compressed air was selected at 117.2 kPa, as this prevents excessive deformation of the PDMS stamp on initial contact with the agarose film. An optimal agarose concentration leads to neither cracks nor incompletely filled structures. To identify this condition, only one parameter changed, while the others were kept at the optimal point (agarose concentration 3%, float delay 60s, heating temperature 70 °C, compressed air pressure 135 kPa). The 3% agarose concentration allows to print structure with the expected shape (**Figure** 2A, middle). When using an agarose concentration at 0.5% or 1%, the film is not stable, which leads to ruptures of the agarose film while imprinting (Figure 2A, left). When the agarose concentration is at 5% the agarose film is too stiff, which does not allow the reproduction of the structures in the film even with exceeded heating temperature (Figure 2A, right). Similarly, by varying heating temperature, float delay time, and compressed air pressures, optimal structures could be obtained at a heating temperature of 70 °C (Figure 2B, middle), float delay of 60s (Figure 2C, middle), and compressed air pressure of 135 kPa (Figure 2D, middle), respectively. A shorter float delay time as well as a lower temperature or pressure lead to incomplete filling of the cavities of the stamp (Figure 2B–D, left).

In contrast, an excessively prolonged float delay, along with an excessive temperature or compressed air pressure, causes the

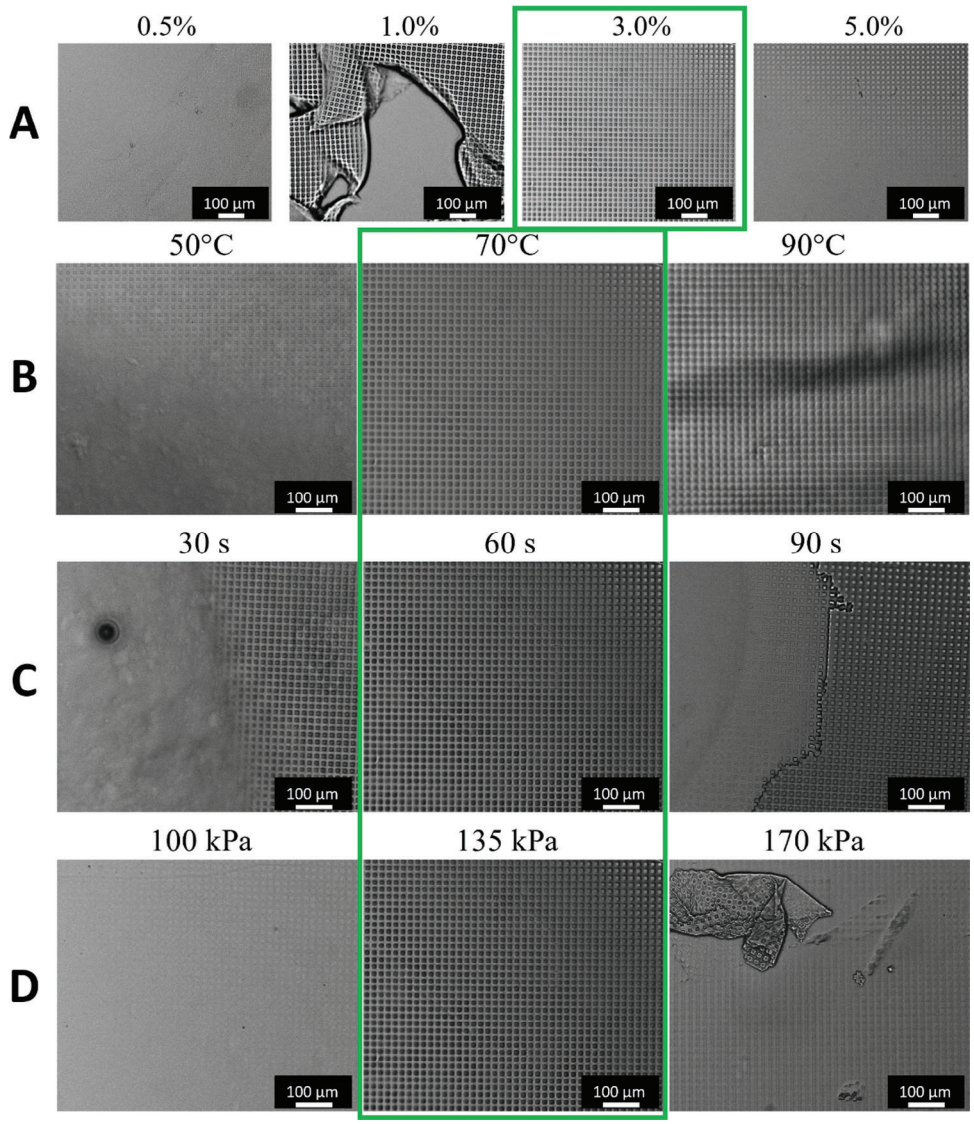

Figure 2. Effect of imprinting parameters on the fabrication of structured agarose patterns. A) Optimization of the agarose concentration: the optimal agarose concentration of 3% leads to neither cracks (A, left) nor incompletely filled structures (A, right). A lower (B) heating temperature, (C) float delay and (D) pressure lead to incompletely filled structures, as too long filling time or too high temperature or pressure leads to cracks and deformation.

disruption and deformation of the agarose film (**Figure** 3B–D, right). This applies to the square structures (Figure 2), but similar behavior can also be found for dot, chain, and pill structures (Figures S1–S4, Supporting Information). Therefore, the optimal values for the printing parameter were identified as a heating temperature of 70 °C, heating time of 180 s, and compressed air pressure of 117.2 kPa resp. 135.3 kPa, a float delay time of 60 s, and a cooling time of 240 s. These parameters were used in all experiments. In summary, to achieve the successful fabrication of micro-/nanostructures on agarose films, a systematic exploration of agarose concentrations ranging from 0.5 to 5% was conducted in water. The formed films with agarose concentrations below 1% exhibited a notable disruption which is attributed to their low stability. In the concentration range of 1 to 2%, successful imprints were observed, albeit with features lacking sharply defined structures. At 3% agarose concentration, the imprinted features demonstrated the highest stability (Figure 2A).

2.2. Characterization of Agarose Film

The viscoelastic behavior and the mechanical characteristics of the 3% agarose film were evaluated by amplitude sweep tests (Figure 3) to determine storage modulus (G'), loss modulus (G''), and vital mechanical properties by constructing a stress-strain curve. Variable oscillatory deformations as a function of strain were systematically applied to the circular agarose discs, facilitating the determination of key mechanical properties and monitoring the variable deformation. Figure 1A shows a direct correlation between stress and strain (deformation), exhibiting the deformation of the agarose gel as the stress intensifies. The

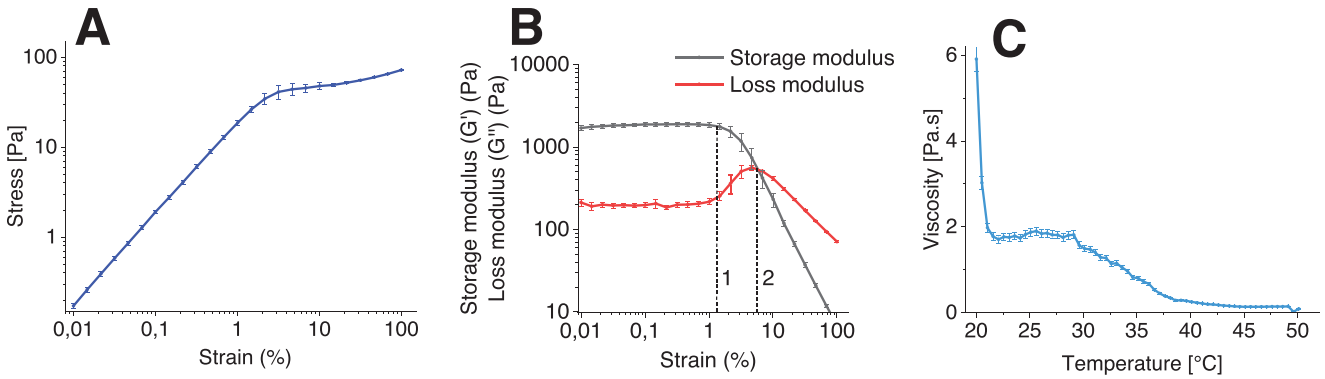

Figure 3. Mechanical properties of 3% agarose film. A) The stress-strain curve shows the variation in the mechanical properties of agarose. B) Representation of amplitude-sweep profile. Storage modulus (black, G') and loss modulus (red, G'') plot concerning varying deformation at 25 °C and constant frequency (f = 1 Hz). Points "1′ and "2′ (in B) correspondingly indicate elastic and viscous state. C) Representation of temperature sweep profile. The G" and G"' curve represents the viscoelastic behavior of the gel. Mean values ± SD were determined from n = 3 repetitions.

elastic region was observed between 0% to 2.17% deformation, while the yield point was at 3.18% deformation. The ultimate strength region was between 5% to 46.4% deformation. The storage modulus serves as a metric for the energy stored and recovered during each cycle, reflecting the material's resilience. It strongly depends on the amplitude of strain, indicating the elastic response to deformation. The loss modulus characterizes the polymer's viscous attributes, representing the energy dissipated during each cycle of the deformation concerning the amplitude of deformation. At lower amplitudes of deformation, storage modulus, and loss modulus indicate linear behavior and are followed by a decrease in their values as the amount of deformation increases. At lower values of strain, that is, between 0% to 2%, the G' exhibited a slight change (Figure 3B, region 1), indicating the elastic behavior of the agarose gel, followed by a gradual decrease indicating the onset of viscous behavior. Conversely, G'' remained constant at lower values of strain and then gradually increased as the amount of strain amplified, indicating the transition from the elastic to the viscous state (Figure 3B, between regions 1 & 2). This trend persisted until a cross-over point where the rate of change in G' surpassed G'', leading to divergence in the moduli (Figure 3B, region 2). The convergence of these curves at the "cross over point" at 8% of deformation signifies a critical transition from elastic to viscous behavior of the material (Figure 3B). The maximum storage- and loss-modulus of the agarose gel were reached at 1878.3 Pa and 563.5 Pa, respectively (Figure 3B). These values indicate the magnitude of storage modulus and loss modulus which display the maximum amount of elastic energy that can be stored and dissipated when the agarose gel is deformed. This intriguing phenomenon of the cross-over point was observed in the amplitude sweep profile, revealing crucial insights about complex viscoelastic behavior and mechanical properties of agarose under variable percentages of deformation or strain. Further, the stress-strain curve shows a linear behavior at lower levels of strain and a non-linear relationship at higher levels (Figure 3A). The material can regain its original shape at a lower amount of strain and eventually might reach its fracture point experiencing plastic deformation. In the G' and G'' curves (Figure 3B), at lower values of strain, the agarose gel exhibited elastic behavior which might be important for the flexibility of platelet storage bags. At the same time, an increase in G'' indicates the viscous behavior of agarose gel, representing fluid-like behavior at a level amount of strain. These mechanical properties are important for the optimization of fabrication parameters and for fine-tuning an enhanced performance in the storage of platelets.

To understand the dynamic viscosity of agarose as a function of temperature, agarose was subjected to varying temperatures between 20 and 50 °C. The temperature sweep profile exhibits an effect of viscosity upon varying the temperature (Figure 3C). The viscosity at 20 °C is 6 Pa·s, indicating that agarose exhibits a viscous behavior. As the temperature increases, the viscosity gradually decreases. At 50 °C, agarose has the lowest viscosity of 0.9 Pa·s, indicating a transition toward more fluid-like behavior. The temperature range between 35 and 50 °C revealed notable changes in viscosity and flow behavior as temperature changed.

2.3. Analysis of Geometries of Imprinted Agarose Patterns

Under optimized conditions, four distinct geometries including dots, chains, pills, and squares were meticulously fabricated. Unpatterned agarose films and bare glass were used as controls. The utilization of Si masters (**Figure 4**, 1st column) facilitated the fabrication of PDMS stamps of dot, chain, pill, and square patterns (Figure 4, 2nd column). Subsequently, these precision-crafted stamps were applied to agarose films under controlled heating and cooling conditions, leading to the imprinting of specific agarose structures (Figure 4, 3rd column).

For a detailed characterization of the imprinted agarose structures, parameters such as width, length, and height of the structures were analyzed through Atomic Force Microscopy (AFM). The presentation of AFM micrographs for each pattern, coupled with their corresponding line profiles, is depicted in Figure 4 (4th column). A comprehensive analysis of structural geometries via line profiles highlighted variations in sizes and heights among the printed structures (**Table 1**). The length of the structures was shortest for dots (2.524 ± 0.214 μm), followed by pills (4.764 ±

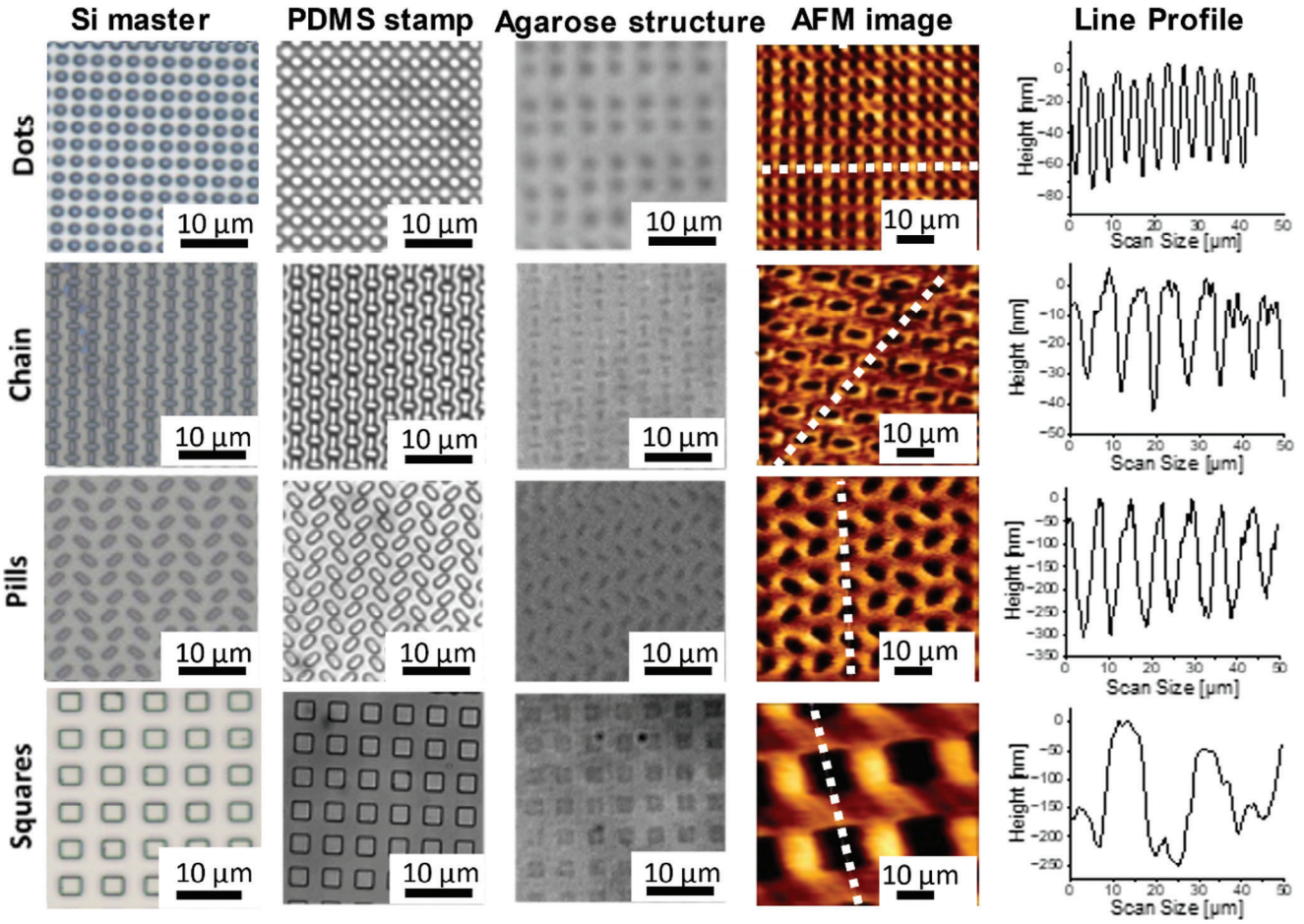

Figure 4. Agarose imprinted structures. (1st column) Si masters featuring distinct patterns including dots, chains, pills, and squares were employed for the fabrication process. (2nd column) The resulting PDMS stamps were meticulously crafted to mirror the geometries of the Si masters. (3rd column) Bright-field images capture the visual representation of the corresponding agarose structures achieved through the application of the generated PDMS stamps. (4th column) AFM images, coupled with their corresponding line profiles, provide a detailed analysis of the sizes and heights of the imprinted structures.

0.327 µm) and chain (4.372 ± 0.376 µm), and longest for squares (12.007 ± 0.657 µm). The feature width varies with the same trend as the height, that is, smallest for dots (2.025 ± 0.150 µm), followed by pills (3.074 ± 0.255 µm) and chain (2.609 ± 0.388 µm), and largest for squares (11.689 ± 0.834 µm). This trend changed when considering structural heights as it was lowest for chains (28 ± 6 nm), followed by dots (60 ± 8 nm), higher for squares (204 ± 42 nm), and highest for pills (280 ± 40 nm). The surface roughness of the glass and un-patterned agarose was obtained by polynomial fits, showing similar values of 10 ± 2 nm and 11 ± 3 nm, respectively. The aspect ratio (= height/width) was correspondingly 0.030 ± 0.004, 0.010 ± 0.005, 0.090 ± 0.020, and 0.020 ± 0.004 for dots, chains, pills, and squares (Table 1). The platelets are expected to respond differently to these imprinted agarose patterns of dissimilar characteristics.

The mean and standard deviation were determined from ≥5 individual features measured on 5 different spots on each sample.

Table 1. Dimensions of the imprinted agarose structures.

Geometry	Length [µm]	Width [µm]	Height/Roughness [µm]	Aspect ratio [height/width]
Dot	2.524 ± 0.214	2.025 ± 0.150	0.060 ± 0.008	0.030 ± 0.004
Chain	4.372 ± 0.376	2.609 ± 0.388	0.028 ± 0.006	0.010 ± 0.005
Pill	4.764 ± 0.327	3.074 ± 0.255	0.280 ± 0.040	0.090 ± 0.020
Square	12.007 ± 0.657	11.689 ± 0.834	0.204 ± 0.042	0.020 ± 0.004
Unpatterned	–	–	0.011 ± 0.003	–
Glass	–	–	0.010 ± 0.002	–

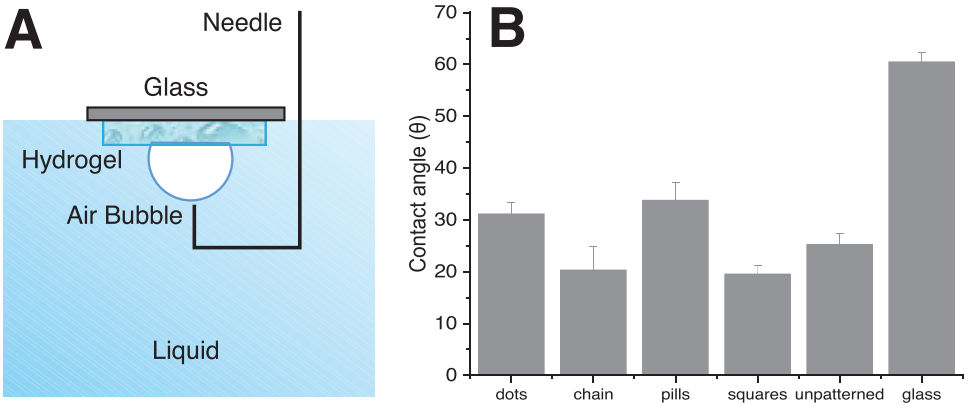

Figure 5. Water contact angles of structured agarose surfaces. A) Schematic illustration of the measurement of sample contact angle through the captive bubble method. B) Hydrophilic properties were observed across all agarose surfaces, as evidenced by consistently lower water contact angles than the glass. The un-patterned agarose surface displayed a decrease in contact angle as compared with dots and pills while chains and squares showed an increase. Mean values ± SD were determined from n = 3 different gel surfaces.

2.4. Surface Wettability Analysis

To understand the wettability characteristics of structured surfaces, their surface contact angles were determined (**Figure** 5A). The structured and unpatterned surfaces demonstrated hydrophilic behavior, evident from contact angles below 30° (Figure 5). The measured contact angle is in line with the results reported previously with consideration of drying state as the determination of contact angle depending on the degree of agarose hydration.[48] Upon closer inspection, a comparison with the unpatterned agarose surface (25.2° ± 2.16°) revealed variations. The dots (31.1° ± 2.1°) and pills (33.8° ± 3.4°) exhibited an increase in contact angles whereas the chains (20.3° ± 4.5°) and squares (19.5° ± 1.8°) resulted in a reduction. In comparison with the glass control surface (60.5° ± 1.7°), the wettability is enhanced in all cases. These changes may lead to differences regarding the anti-fouling properties of the surface.

2.5. Response of Platelets on Agarose Micro/Nanostructures

To elucidate the impact of agarose micro/nanostructures on platelet adhesion, platelets were incubated on the patterned surfaces. Optical microscope imaging, utilizing both bright field (**Figure** 6A, top) and Confocal Laser Scanning Microscopy (CLSM) (Figure 6A, bottom), captured the platelet adhesion on each sample with distinct geometries. For CLSM imaging, the surface-expressed protein CD42a on platelet membranes which acts as a platelet-specific membrane marker were stained with anti-CD42a FITC antibodies (green, Figure 6A, bottom) while their actin fibers were stained by DY590 phalloidin indicating the activation and formation of filopodia and lamellipodia of the platelets (red, Figure 6A, bottom). Non-activated platelets on structured surfaces keep their round shape (Figure 6B) whereas activated platelets on the glass highlights the formation of lamellipodia and filopodia upon activation (Figure 6C).

CLSM micrographs show a robust activation of platelets on the glass surface, characterized by the formation of filopodia and lamellipodia, leading to a discernible alteration in the original platelet shape after 1 h of incubation. Conversely, such phenomena were not observed on agarose surfaces (Figure 6A). ImageJ was used for quantifying the number of adhered platelets, revealing a significantly higher platelet count on glass compared to other agarose-based surfaces (Figure 6B). Notably, among all agarose structured surfaces, the pills and dots exhibited the lowest number of adhered platelets. To unravel the influence of geometries on platelet adhesion, a closer examination by comparing the number of platelets with the wettability of differently structured surfaces was examined. It can be seen that dot-, as well as pill-shaped surfaces, show a reduced platelet amount. In comparison with square and chain-shaped structures, which show an increased number of platelets, the contact angles for dots and pill structures are higher. This leads to the conclusion that both the contact angle and feature of the structures play a role in the reduction of platelet adhesion.

2.6. Response of Platelets on Agarose Structure at Different Contacting Times

In the context of platelet storage applications, the development of bag surfaces capable of preventing platelet adhesion over extended periods is of paramount importance to mitigate platelet-surface activation and potential damage. Here, we systematically investigate the efficacy of agarose structures in preventing platelet adhesion over a 4-h timeframe. Platelets were incubated on the surfaces for varying durations-15 min, 1 h, and 4 h before fixation and staining for subsequent imaging. The platelet count was quantified across three different structured gels for each geometry, incorporating assessments from multiple platelet donors. Our findings consistently indicate that, at each time point, the unpatterned surface exhibited the highest number of adhered platelets compared to the patterned ones (**Figure** 7).

Notably, an observable increase in platelet adhesion to the unpatterned and square-shaped samples was evident after 4-h of contact, whereas other topographies exhibited lower cell

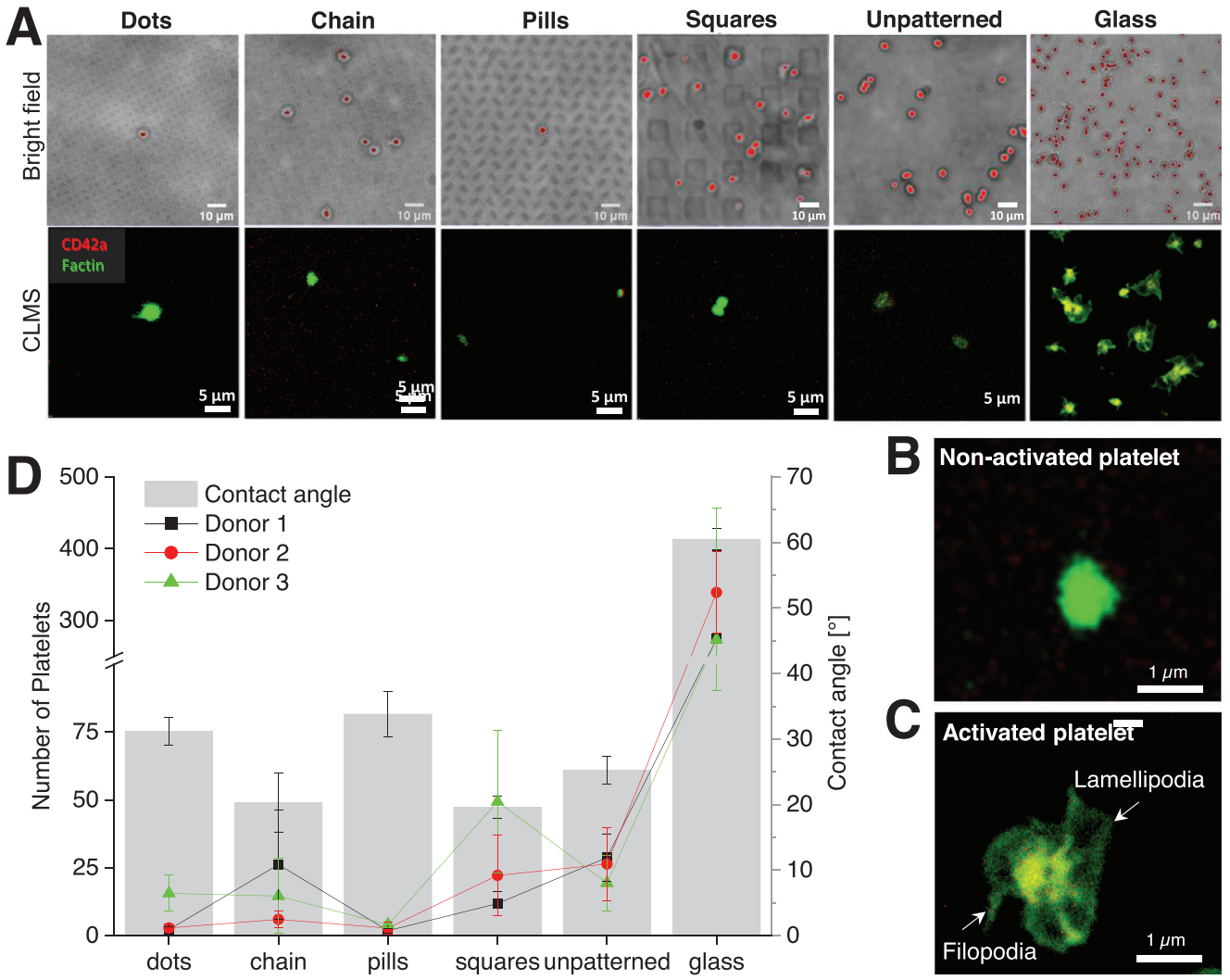

Figure 6. Response of platelets on imprinted agarose surfaces after 60 min incubation. A, top) Bright-field images with the red marks indicate the ImageJ markers for counting of platelets. A, bottom) CLSM images illustrate the variations in both the number of adhered platelets and their morphologies, revealing the influence of underlying surface properties; surface-expressed protein CD42a on platelet membranes were stained with anti-CD42a FITC antibodies (Green) and actin fibers were stained with DY590 phalloidin (Red). CLSM images are overlays of both green and red channels, resulting in a yellow color (A, bottom). B) Non-activated platelet keeps its round shape whereas (C) activated platelet on the glass highlights the formation of lamellipodia and filopodia upon activation. D) The quantification reveals a significantly lower number of platelets adhering to respective geometries after 1 h of incubation when compared to glass. The correlation with the contact angle of the structures (gray bars), provides insights into the relationship between contact angle and platelet adhesion. Mean values ± SD were determined from n = 3 donors.

adhesion levels (Figure 7). At 15 min incubation time, in comparison to glass, the agarose surfaces strongly inhibited platelet adhesion (Figure 7). The unpatterned surfaces showed a higher number of platelet adhesion than the structured surfaces. At an incubation time of 4 h (Figure 7), multiple platelets adhered together on the glass did not allow for a precise counting of platelet numbers (marked as >500). Since the glass serves as a control while sample evaporation also causes platelet activation, we did not extend the incubation time to longer than 4 h. The adhered platelets increased on unpatterned surfaces, squares, and chains but did not significantly change on dots and especially on pills (Figure 7).

This emphasizes the potential of dots, especially, pill structures in designing anti-platelet adhesion surfaces. Overall, the results underscore the efficacy of agarose-based surfaces in the prevention of platelet adhesion, even after 4-h of contact. This holds promising implications for the design of platelet storage systems utilizing agarose micro/nano pill/dot structures.

3. Discussion

Our focus revolves around the breakthrough potential of engineered agarose micro/nanostructures in overcoming critical limitations associated with platelet storage. The study's primary objective is to address the pervasive issue of unwanted platelet-bag activation during storage, a factor significantly restricting the product shelf life to less than 72 h and resulting in considerable wastage and elevated costs. We have previously demonstrated

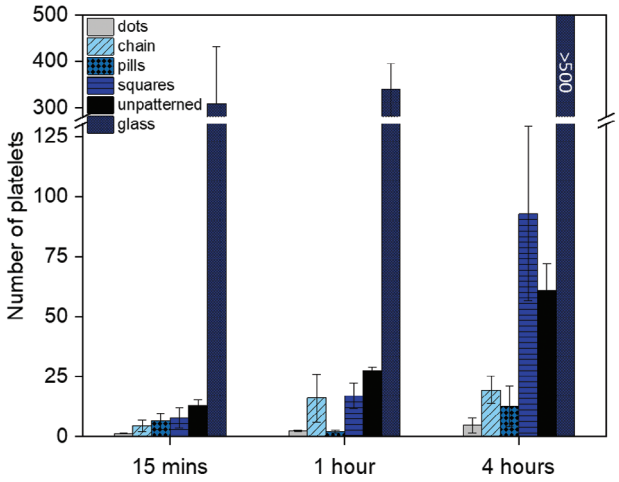

Figure 7. Platelet adhesion on structured surfaces at different incubation times. (A) At 15 min incubation time, the highest number of platelets adhered on glass, followed by un-patterned agarose, and the lowest on structured surfaces were observed. At longer incubation time of 1 h or 4 h (platelets aggregated that did not allow to count correctly platelet numbers marked as >500) the adhered platelets significantly increased on un-patterned surface, squares, and chains but no significant changes on dots, especially pills. Mean values ± SD were determined from n = 2 donors.

that agarose film could strongly prevent platelet adhesion.[46] In this study, we further improve the anti-platelet adhesion properties by fabricating well-defined agarose patterns of different geometries. T-NIL technology for producing agarose surface structures including dot, chain, pill, and square features has been successfully implemented. The structured surfaces displayed exceptional stability and hydrophilic behavior, effectively thwarting platelet adhesion compared to the unpatterned agarose film. Notably, the pill-shaped structures maintained their anti-platelet adhesion properties even after prolonged contact for up to 4 h. The nuanced interplay of shape, height, and size of structures influenced the degree of platelet adhesion. As the agarose layer is ≈1 mm thick, it remains sufficiently thick even after the nanoimprinting process, ensuring that the glass substrate is completely covered by a residual layer of agarose. This thickness also eliminates the possibility of mechanical differences in the cavities affecting platelet behavior, as the platelets interact with the structured agarose surface only. The fabricated surfaces emerge as promising for revolutionizing platelet storage practices, providing valuable insights into "green" biomaterials research and underscoring the considerable potential of engineered agarose surfaces in advancing biomedical applications.

The successful fabrication of agarose micro/nanostructures through T-NIL stands as a pivotal achievement in our study, marking the inception of a systematic exploration into the capabilities and applications of these engineered structures. Central to this endeavor was the optimization of agarose concentration, transitioning from 1% for film formation in our prior work[46] to 3% in this study, a crucial factor in establishing a robust imprinting procedure. Analysis of mechanical properties shows that the 3% agarose film exhibited viscoelastic or fluid-like behavior, indicating its flexibility which is an important factor for the development of platelet storage bags. Also, the printing parameters such as float delay, compressed air pressure, and heating temperature are strongly influenced by the integrity of the structured agarose. Inappropriate printing parameter values can result in poor shape fidelity of microstructures on agarose gel. These parameters aid in maintaining optimum material viscosity, adjusting flow behavior to fill the mold or stamp features, and elasticity of material while imprinting. Excessively low or high parameter values result in a loss of elasticity and flow properties as the material shows a linear relation between applied stress and deformation only in a particular range of strain. Optimizing the float delay and heating temperature ensures the generation of ideal imprinted patterns on the surface of agarose gel and prevents plastic deformation of agarose.

Rheological characterization revealed crucial insights about viscoelastic behavior and stress-strain characteristics of agarose which is important for the optimization of the fabrication parameters and accomplishing high-fidelity structures. Furthermore, stress-strain characterization provides insights into the influence of various levels of strain on the agarose gel. It aids in understanding the maximum amount of stress that a material can withstand while retaining its elastic properties. This analysis of key mechanical attributes like stiffness, or temperature-dependent viscosity not only aids in optimizing printing parameters but also reveals more about material flexibility and durability. These tests provide insight about material strength and stability which is a crucial consideration while transporting and handling the platelet storage bags. The selection of an optimal agarose concentration (3%) and the fine-tuning of imprinting parameters such as heating temperature and imprinting pressure (Figure 3) provided a critical basis for ensuring superior stability and reproducibility in the fabricated structures, forming the base for the multifaceted exploration that ensued.

The suitable agarose concentration (3%) contributes to stiffness that is neither too hard (5%) nor too soft (0.5% and 1%) for optimal imprinting of the structures. A filling time that is too short leads to incompletely filled structures, while a filling time that is too long leads to increased adhesion and thus cracks. Hence, an optimal filling time is necessary for the complete filling of the structures. It is known that an increased temperature leads to a reduced viscosity of the agarose (Figure 3C). If the temperature is too low, the agarose is still too stiff and it is therefore not possible to mold the structure. If the temperature is too high, the agarose becomes too soft and the residual layer is deformed, resulting in the formation of a valley due to the imprint pressure. It is not possible to reduce the stamping pressure, as too low a pressure leads to unstable filling, and therefore, not to the desired imprint. If the stamping pressure is too high, valleys are formed as well as tears and cracks in the agarose The reproducibility of the imprint process shows its evident in the homogeneous patterns as validated by AFM micrographs and line profiles (Figure 4, Table 1).

The investigation of platelet responses to agarose structures uncovered their potential to prevent adhesion, particularly in prolonged storage scenarios. Utilizing optical and CLSM imaging, alongside quantification, we were able to underscore the efficacy of structured agarose surfaces in impeding platelet adhesion. Microscopic imaging revealed an absence of platelet activation on agarose surfaces, contrasting markedly with the glass surfaces exhibiting discernible spiky filopodia and planar lamellopodia. Importantly, the platelet adhesion on the structured

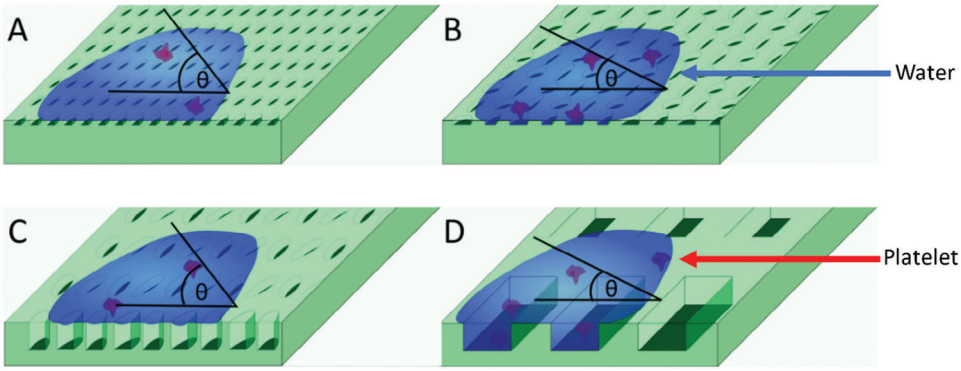

Figure 8. Structural features alter the contact angle of water and the agarose film at interfaces. Wetting behavior depends on surface structures such as (A) dots, (B) chains, (C) pills, and (D) squares. Surfaces represent the Cassie-Baxter (A, C) and Wenzel states (B, D) corresponding to high and low contact angles.

surfaces remained remarkably subdued relative to the unstructured surface. This effect is in contrast to the less hydrophilic glass that attracts more platelets (Figure 6B). The dissimilar degree of platelet adhesion on the investigated structures is attributed to the modification of surfaces by each specific structural feature. First, surface wettability, a critical aspect influencing various applications is investigated through contact angle measurements. The amount of platelets is strongly dependent on the water contact angle. The contact angle on dot and pill structured surfaces is slightly higher than on chain, square, and unpatterned surfaces. From previous work, it is known that surfaces with low contact angles (hydrophilic surfaces) are exposed with superior anti-biofouling properties that combat microorganism attachment.[46,49] For agarose structured surfaces, this principle is not applicable as dot and pill structured surfaces show higher contact angles but a lower amount of bound platelets. Here, another principle relating to structural geometry may play a role. The pill-shaped structures show the highest height with ≈280 nm and relatively small dimensions (width ≈ 3 µm, length ≈ 5 µm), exhibiting robust prevention of platelet adhesion. This anti-adhesive efficacy endured even after extended platelet-surface contact for up to 4 h. In contrast, chain and square structures with lower heights and larger dimensions failed to replicate this remarkable anti-adhesive capability after 4-h incubation. Here, different wetting behaviors can occur with microstructures. In particular, it can be distinguished between the Cassie-Baxter- and the Wenzel state where the Cassie-Baxter state leads to a comparatively higher contact angle. It is known that the Cassie-Baxter-state can be forced to the Wenzel state when the energy barrier is overcome (**Figure 8**).[50] This energy barrier strongly depends on the interspacing of the structures.[51] The breaking pressure ΔP of the water meniscus which leads to the transition between Cassie-Bater to Wenzel-state depends on:

$$\Delta P = \frac{2\gamma}{\frac{x}{2}} \tag{1}$$

whereby x is the interspacing of the structures and γ the surface tension of the water.

In contrast to the gapping area, the contacting area for the dot and pill structures seems sufficient for holding the Cassie-Baxter state longer than the square structures. This is due to the fact that the relatively wide gaps of squares lead to a collapse of the Cassi-Baxter state the quickest. Also, the chain structures show, along the x-axis, relatively large gaps with only small pitches which have therefore reduced contacting areas to water, leading to a lower ΔP and a quicker transition from the Cassie-Baxter state to the Wenzel state. Besides the intrinsic pressure ΔP, other effects can lead to the crashing of the Cassie Baxter state, for example, condensation, evaporation, diffusion of air into the liquid, fluid flow along the interface, and even cavitation.[52] Additionally, surface roughness that is induced by structures of different features and sizes can also affect the ability of platelet adhesion. For example, the large size and wide interspace of squares promote the trapping of platelets among structures whereas the small size and narrow interspacing of others cannot trap cells, and thus, effectively prevent platelet adhesion. Further, the shape of structures also plays a role, for example, the sharp edges of squares may trigger platelet activation and adhesion during rolling while round edges of other structures may not. This is due to the fact that platelets are highly sensitive as they are activated even under high flow[53] or when contacting hard surfaces.[54,55] It is notable to mention that platelets can only contact the surface and start activation in areas where the surface is contacting the liquid. Therefore, pill and dot structures have a reduced area for contacting platelets (Figure 8). This explains the higher amount of platelets bound over time for large interspacing structures, especially for squares. Also after a short time, structures with lower contact angles show an increased platelet adhesion. This amount of platelets can be reached by the structures with high contact angles (pills and dots) after a longer period (≈1 h). After 4 h, the number of platelets bound to the dot structures reaches the amount of platelets bound to squares after 1 h.

Our findings underscore that the pivotal factors influencing platelet adhesion to structured surfaces extend beyond shape alone; height, width, and size also play integral roles in this dynamic. This stands as a testament to the exceptional thrombocompatibility inherent to agarose structured surfaces. The distinct platelet responses to different geometries further emphasized the critical role played by wettability in governing cellular interactions, paving the way for tailored surfaces with controlled cellular behavior. Revisiting the platelet investigations

underscored and reaffirmed prior insights, emphasizing the intrinsic trait of agarose-based materials to elicit diminished platelet adhesion and activation compared to alternative biomaterials.

In comparison with commercially available resins, agarose shows much stronger anti-platelet adhesion properties.[46,56] In alignment with past in vivo demonstrations, agarose-based materials maintained a non-thrombogenic profile, refraining from promoting clotting in animal models or medical devices.[44] The comprehensive integration of these findings offers a nuanced understanding of how agarose micro/nanostructures can be engineered for advanced biomedical applications. Spanning the realms of fabrication, characterization, and biological responses, our research underscores the potential for tailored functionalities in applications ranging from tissue engineering to medical devices and regenerative medicine.

Our results also highlight avenues for further exploration. Long-term stability considerations and a deeper investigation into the molecular interactions at the interface of structured surfaces and platelets emerge as promising directions for continued research. Agarose is generally stable at room temperature and maintains its structural integrity only under a particular range of temperature and stress. It exhibits excellent mechanical strength and swellability. Hydrophilic surfaces can inhibit the thrombosis cascade as they can resist the adsorption of fibrinogen which results in less platelet adhesion.[57] Swelling leads to the formation of a hydrated smooth surface and limits exposure of binding sites on agarose gel which can reduce platelet adhesion and activation.[58] However, agarose is not suitable for long-term storage as it can be challenging to maintain its structural integrity and durability due to its limited flexibility. It can be observed from mechanical characterization that, agarose is brittle and is flexible only under a short range of deformation. Also, due to its gel-like consistency agarose is less durable as surface coating and can detach from the surface in long-term usage. Nevertheless, we demonstrated that the fabricated agarose films show a viscoelastic behavior and can reshape up to 15% stretching (Figure 3B). This is in line with the findings by Hernandez et. al who reported stretching of agarose up to 15.8%. Therefore, while bending and handling these surface coatings can be taken into consideration as stable.[59] This stability is also given at room temperature (Figure 3C). Even when agarose molecules are leaking, due to its biocompatibility no danger is to be assumed from interaction with the body.[44,60] To further ensure a stable bond between the film and the bag, Grubenhofer patented a surface bonding technique using ester groups, to fix the agarose to plastic bags which is a promising approach for further investigations.[61] Its durability can be enhanced by combining it with other materials or by chemical modifications.[44] These future research directions hold the potential to refine our understanding of structured agarose surfaces and extend their applications into novel realms within the biomedical field. Our interdisciplinary study significantly contributes to the evolving landscape of biomaterials. The intricacies embedded in agarose micro/nanostructures offer a versatile platform with far-reaching implications for various biomedical applications. This research serves as a foundational step, unlocking the potential of structured agarose surfaces and laying the groundwork for enhanced medical technologies and therapeutic interventions. The contemporary challenges in platelet storage, encompassing issues of both platelet activation and bacterial contamination,[9,11] underscore the pressing need for the development of agarose-based materials in transfusion medicine. Several factors influence the shelf life of stored platelets, including pH, temperature, gas exchange, bacterial contamination, and storage material.[62] The widely used (Di(2-ethylhexyl)-phthalat)-PVC containers accumulate carbon dioxide and lactic acid, resulting in a rapid decline of pH with subsequent poor clinical outcomes. Thus, DEHP-free and high permeability bags to facilitate O_2 transport have been introduced to several markets.[19] For example, polyolefin bags (a blend of polypropylene and ethylene butylene copolymer and polystyrene) do not contain plasticizers while Trioctyl trimellitate (TOTM) plasticized PVC containers show intermediate leaching. These special bags allow storage of platelets for up to 7 days because of their ability to keep pH constant. However, TOTM-PVC containers also reduced the recovery of up to $45.6 \pm 7.8\%$ on day-7 compared to $71.0 \pm 9.6\%$ on day-3 storage. Nevertheless, these bags are provided only by some services.[25,63] We speculate that our agarose structured surfaces exhibit several advantages. First, the agarose gel is composed of large molecules as a network which may entrap CO_2 during storage. Second, the introduction of structures significantly increases the area of the inside surface of the bags which enhance the CO_2 entrapping process. The mentioned advantages, however, require further investigation for confirmation. In the most recent development, Stubbs et al aimed to extend the platelet storage period above 10 days by keeping them in cold conditions, meaning that a longer period for keeping platelets in the bags is required.[64] Unfortunately, the long-time contact, especially under agitation will increase plasticizer leaching.[65,66] The existence of the agarose layer can effectively prevent a direct contact of the platelet sample with the plastic bag underneath, resulting in a minimization of plasticizer leaching. Regarding temperature, the agarose matrix does not prevent or slow down the entire bag from reaching the desired temperatures.[9]

Given the recognition of pill-shaped structured surfaces as potential candidates for advanced platelet-contacting devices, the subsequent phase of investigation should pivot toward incorporating antimicrobial elements into these surfaces. As factors that govern microbial attachment involve different types of physical-chemical interactions and biological processes,[67] materials such as silver nanoparticles, antibiotic-embedded substances, or other antimicrobial agents can be introduced into agarose-based materials to augment their ability to resist bacterial growth. Encouragingly, our successful integration of iron oxide nanoparticles, which exhibit antimicrobial properties, into agarose gels demonstrated the feasibility of introducing antimicrobial elements without inducing platelet activation.[46] This established protocol serves as a foundation, offering a basis for modification and adjustment to effectively incorporate diverse antimicrobial agents into agarose gels before the imprinting process. The World Health Organization has highlighted the impact of bacterial contamination, affecting ≈1% of pooled units,[2] and the consequential formation of bacterial biofilms within storage bags. This biofilm formation not only decreases the visibility of floating bacteria but also poses challenges for accurate pathogen detection, resulting in potential false-negative results in bacterial tests. In a recent tragic incident, a splenectomized patient with leukemia succumbed to sepsis caused by a platelet unit contami-

nated with Staphylococcus epidermidis.[68] This underscores the critical need for the development of bifunctional materials capable of addressing both bacterial contamination and platelet dysfunction during storage, offering a vital solution to enhance the safety and efficacy of platelet concentrates.

4. Conclusion

Our study delves into the critical challenges posed by current platelet storage bags, particularly concerning platelet activation, adhesion, and bioactive substance release during storage. These limitations emphasize the necessity for innovative solutions to enhance platelet-bag interactions and enable prolonged storage without compromising platelet integrity. Engineered agarose micro/nanostructures, especially, pill-shaped features by thermal nanoimprint lithography, reveal promising anti-adhesive properties for platelets. These structures exhibit high stability, great hydrophilic behavior, and surprising efficacy in preventing platelet adhesion even during an extended platelet-contact time of up to 4 h. Our findings underscore that the effectiveness in preventing platelet adhesion is not solely dependent on shape; rather, the size and height of the structure also play pivotal roles. These findings underscore the potential of engineered agarose surfaces for revolutionizing platelet storage technology. This comprehensive study not only contributes valuable insights to biomaterials research but also lays the groundwork for future advancements in biomedical applications, including improved platelet storage systems and enhanced transfusion outcomes.

5. Experimental Section

Ethics: The use of blood obtained from healthy volunteers was approved by the ethics board at the Thüringen Köperschaft des öffentlichen Rechts, Landeszahnärztekammer Thüringen, Germany. The methods were carried out accordingly with the approved guidelines.

Preparation of Agarose: Before imprinting, agarose films were prepared by adding 3% agarose (Mw: 120 kDa; Lonza, Cologne, Germany) into preheated Milli-Q water and stirring at 500 rpm and 75 °C. The agarose solution (1 mL) was cast in a mold made out of the silicone elastomer Sylgard 184 (Dow Corning, Midland USA) as circular discs of ≈8 mm in diameter with a thickness of 1 mm on glass at room temperature. To avoid air bubbles, the gel was poured slowly into the mold, followed by gentle tapping to eliminate any air entrapment. Consequently, a cooling time of 30 min was given to cool down and form the gel.

Rheological Characterization of Agarose Film: The rheological characterization of agarose 3% was performed by using Anton Paar MCR 502 (Anton Paar GmbH, Graz; Austria), equipped with RheoCompass software and parallel plate measuring system (D-PP15 tool) for controlled deformation. A parallel plate system was used for rheological measurements. It is suitable for measuring the rheological behavior of gels or soft materials. An amount of 200 µL agarose was added to the plate for each test. The viscoelastic and mechanical behavior of agarose was determined by using an amplitude sweep test. The effect of the flow behavior of agarose gel upon changing the temperature was determined by using a temperature ramp test. In this test, the storage modulus (G') and loss modulus (G'') of agarose hydrogel were determined under varying amounts of deformations on the agarose gel placed between two parallel plates. Additionally, a stress-strain curve was constructed to evaluate the mechanical behavior of agarose gel comprehensively. A systematic variation in the amount of strain enabled us to capture crucial mechanical properties such as elasticity, yield point, ultimate strength, and fracture point of the material. The material was deformed at a constant frequency (f = 1 Hz) and temperature (25 °C) while varying the oscillatory deformation as a function of strain in the range of 0% and 100% was investigated. In the temperature ramp test, the viscosity or flow behavior change was examined by varying the temperature from 20 to 50 °C. The temperature was ramped in 2 °C s^{-1} Steps. This test allowed for optimizing the printing parameters and provided information on the thermal stability of agarose over a range between 20 °C to 50 °C, data analysis was carried out using Origin 2023b (OriginLab Corporation, Northampton, MA, USA).

Fabrication of Stamps: Commercial silicon (Si) masters with four topographies, namely dot, chain, pill, and square (GeSiM GmbH, Germany) were selected for the fabrication of corresponding PDMS stamps. The silicone elastomer Sylgard 184 (Dow Corning, Midland, USA) was mixed: with 10 parts base and one part curing agent and stirred for 2 min in a glass container. The glass container was placed in an exsiccator and degassed at room temperature under a low vacuum. The degassed PDMS was then sucked into a syringe and prepared for use. Meanwhile, the Si master was placed in the central cavity of the aluminum block. After that, a teflon spacer was added on top of the Si-Master. The PDMS was then filled in the groove of the polycarbonate stamp holder. The polymethyl methacrylate (PMMA) plug was pushed into the polycarbonate cylinder to ensure the formation of a uniform PDMS layer thickness, and both were placed in the casting station over the existing master and spacer assemblies before fastening. Subsequently, PDMS was injected into the inlet port until the liquid came out from the opposite side. Then, the set-up was placed in an oven at 65 °C for 4 h for PDMS to crosslink. With the help of a scalpel, leaked PDMS was scraped. The demolding process was completed by carefully detaching the master from the stamp surface. Finally, the PMMA plug was gently pulled out of the stamp body. The stamps were stored in a clean, closed glass container to avoid contamination for later use within 4 weeks.

Imprinting of Agarose Structures: The imprinting process was carried out using a Microcontact-Printing System (µCP 3.0, GeSiM GmbH, Germany). The PDMS fabricated stamps were picked up by the stamp holder. The films were assembled on the substrate holders, and the imprinting was conducted using the µ-CP control software that allows entering parameters like heating temperature, heat delay, cooling time, initial and final stamping pressure, etc. The stamp was pressed onto the heated agarose films until the agarose was cooled to room temperature. After the agarose was cooled the PDMS stamp was lifted up and detached from the structured agarose.

Imaging of Structured Surfaces by Atomic Force Microscopy: The imprinted patterns were imaged using Atomic force microscopy (AFM) (JPK NanoWizard 3, Berlin, Germany). AFM was used in force modulation mode to acquire the topographical scans. The images were captured at a line rate of 2 Hz and a resolution of 128 × 128 pixels for all samples. A Mikromasch cantilever (HQ: CSC38/tipless/No Al) with a nominal spring constant value of 0.09 N m^{-1} was used. A scan size of 100 × 100 μm^2 was set to image the samples at 5 different regions. Using JPK Nanowizard4 software, line profiles of the features were obtained by selecting the image cross-section option to compute the size of each printed feature.

Water Contact Angle: The water contact angle of the glass surface and agarose films (patterned and unpatterned) was measured with the OCA 15+ system (DataPhysics Instruments GmbH, Filderstadt, Germany) by using the captive bubble method. This method is particularly advantageous when dealing with surfaces with high surface-free energy, especially to avoid the drying of hydrogels during measurement. A small air bubble with a volume of 3 µL was injected beneath the sample, which was placed facing downward, at a dosing rate of 1 µL/s. All samples with different geometries were probed with three air bubbles at different positions. The calculation of contact angles using the ellipse fitting method was done by OCA 15+ software (DataPhysics Instruments GmbH, Filderstadt, Germany).

Response of Platelets on Structured Surfaces: Platelets were isolated from the whole blood following our previous protocol.[34,60,69,70] To generate a monolayer of single platelets (even on bare glass as a control) for accurate counting and platelet area assessment, a low platelet concentration of 30 000/µL was used as described previously.[40] Platelets were incubated on the surfaces for different periods including 15 min, 1 h, and

4 h at room temperature which mimics the actual scenario during platelet storage.[9] Unbound platelets were removed by rinsing with phosphate-buffered saline (PBS), and the platelets were fixed using 4% paraformaldehyde (PFA) for 30 min. To obtain CLSM micrographs, the fixed platelets were stained for 1 h with 0.1 µg mL^{-1} anti-CD42a FITC antibodies (Dianova GmbH, Hamburg, Germany). The unbound dye was then washed off the sample twice with PBS. After that, samples were incubated for 10 min in permeable buffer before being incubated for 45 min at RT (23 °C) in the dark with phalloidin DY590 (Mobitec GmbH, Göttingen, Germany) (1:20 dilution). At RT in the dark, samples were examined using a confocal laser scanning microscope, the Zeiss LSM710 (Carl Zeiss, Gottingen, Germany). Using a 20× and 63× objective, the green fluorescent signal was acquired using the excitation/emission wavelengths = 488/520 nm and the red fluorescent signal was acquired using the excitation/emission wavelengths = 580/599 nm, respectively.

The samples were then imaged under a brightfield microscope with 40x magnification. The images were analyzed using ImageJ software, following a standardized processing workflow. First, the images were imported, and the "Adjust toolbar" was used to select the "Threshold" function. The "Auto threshold" option was applied to isolate platelet structures, and the "Apply" function finalized the adjustment. To quantify the platelet spread, the "Analyze Particles" tool was employed. Quantification involved measuring particles by filtering the area of platelets between 1 and 10 μm^2 within a surface area of 315 × 237 μm^2. This process enabled precise measurement of the spread area and accurate counting of individual adhered platelets across the image. The quantification on glass was approximate in the case of platelet aggregates. The platelets from three donors were used for the 1-h independent experiments and two donors for the time-dependent studies.

Statistical Analysis: To analyze the data all statistical analysis was carried out using origin. The mechanical properties of 3% agarose film were determined by averaging three repeats and calculating the standard deviations. The dimensions of the imprinted agarose structures are the mean and standard deviation of at least 5 individual features measured on 5 different spots on each sample. The water contact angle measurements were carried out using three independent gel surfaces with three repeating the measurements on each sample. The mean and standard deviations were calculated accordingly. For the 1-h independent experiments, the platelets from three donors were used. Each donor was applied to three different surfaces. On each surface, three images were taken. The mean and standard deviation of each donor was calculated and displayed accordingly (Figure 6). For the time-dependent studies, two donors were applied individually on three different gel surfaces. On each of these surfaces, three images were taken. The platelet count was averaged and the mean and standard deviation were calculated accordingly and displayed as error bars (Figure 7).

Supporting Information

Supporting Information is available from the Wiley Online Library or from the author.

Acknowledgements

G.A., M.S., D.M., and T.-H.N. acknowledge the support of the Freistaat Thüringen (Thüringer Ministerium für Wirtschaft, Wissenschaft und Digitale Gesellschaft, TMWWDG, Germany). T.-H.N. acknowledges the partial support of the German Research Foundation (DFG) within the project (Nr. 469240103).

Conflict of Interest

The authors declare no conflict of interest.

Author Contributions

G.A. and M.S. contributed equally to this work. G.A. developed the methodology, performed T-NIL experiments and platelet experiments, analyzed the data, discussed the results, and wrote the original draft of the manuscript. M.S. performed T-NIL optimization and some platelet adhesion experiments, analyzed and discussed the results, and wrote the manuscript. D.M. characterized the mechanical properties of agarose film and wrote the manuscript. H.D. discussed the results, partially supervised the model development, and revised the manuscript. T.H.N developed the study concept, discussed the results, performed the supervision, acquired the fundings, and wrote the manuscript. All authors have read and agreed to the final version of the manuscript.

Data Availability Statement

The data that support the findings of this study are available on request from the corresponding author. The data are not publicly available due to privacy or ethical restrictions.

Keywords

adhesion, Agarose, height, imprint, micro/nanostructures, platelet, shape, size

Received: August 3, 2024
Revised: October 21, 2024
Published online:

[1] G. Vit, H. Klüter, P. Wuchter, *J. Labor. Med.* **2020**, *44*, 285.
[2] WHO, *Blood safety and availability* **2022**.
[3] A. P. Cap, P. C. Spinella, *Transfusion* **2017**, *57*, 2817.
[4] K. Nagai, H. N., Y. Koga, H. Harada, C. Yakushiji, E. Kino, M. Tokunaga, H. Yamaoka, Y. Miyazaki, *Blood* **2018**, *132*, 1261.
[5] V. T. DeVita, Jr., R. C. Young, G. P. Canellos, *Cancer* **1975**, *35*, 98.
[6] A. W. Flint, Z. K. McQuilten, G. Irwin, K. Rushford, H. E. Haysom, E. M. Wood, *Transfus. Med. Rev.* **2020**, *34*, 42.
[7] The University of Mississippi, M. c., Blood Product Utilization Guidelines.
[8] D. W. C. Dekkers, I. M. De Cuyper, P. F. Van Der Meer, A. J. Verhoeven, D. De Korte, *Transfusion* **2007**, *47*, 1889.
[9] C. Aubron, A. W. J. Flint, Y. Ozier, Z. McQuilten, *Crit. Care* **2018**, *22*, 185.
[10] J. Sahler, K. Grimshaw, S. L. Spinelli, M. A. Refaai, R. P. Phipps, N. Blumberg, *Drug Discov. Today: Disease Mech.* **2011**, *8*, e9.
[11] J. H. Levy, M. D. Neal, J. H. Herman, *Crit. Care* **2018**, *22*, 271.
[12] M. Arman, K. Krauel, D. O. Tilley, C. Weber, D. Cox, A. Greinacher, S. W. Kerrigan, S. P. Watson, *Blood* **2014**, *123*, 3166.
[13] J. Rivera, M. L. Lozano, L. Navarro-Núñez, V. Vicente García, *Haematologica* **2009**, *94*, 700.
[14] E. M. Golebiewska, A. W. Poole, *Blood Rev.* **2015**, *29*, 153.
[15] P. F. Van Der Meer, J. L. Kerkhoffs, J. Curvers, J. Scharenberg, D. De Korte, A. Brand, J. De Wildt-Eggen, *Vox Sang.* **2010**, *98*, 517.
[16] M. Weber, H. Steinle, S. Golombek, L. Hann, C. Schlensak, H. P. Wendel, M. Avci-Adali, *Front. Bioeng. Biotechnol.* **2018**, *6*, 99.
[17] B. D. Ratner, *Biomaterials* **2007**, *28*, 5144.
[18] C. V. Prowse, D. de Korte, J. R. Hess, P. F. van der Meer, *Vox Sang.* **2014**, *106*, 1.
[19] P. F. van der Meer, D. de Korte, *Transfus. Apher. Sci.* **2011**, *44*, 297.
[20] G. Latini, M. Ferri, F. Chiellini, *Curr. Med. Chem.* **2010**, *17*, 2979.
[21] R. J. Jaeger, R. J. Rubin, *Science* **1970**, *170*, 460.

[22] H. M. Koch, M. Wittassek, T. Bruning, J. Angerer, U. Heudorf, *Int. J. Hyg. Environ. Health* **2011**, *214*, 188.
[23] M. Romero-Franco, R. U. Hernandez-Ramirez, A. M. Calafat, M. E. Cebrian, L. L. Needham, S. Teitelbaum, M. S. Wolff, L. Lopez-Carrillo, *Environ. Int.* **2011**, *37*, 867.
[24] European Commission. Directorate General for Health and Consumers., Opinion on the safety of medical devices containing DEHP plasticized PVC or other plasticizers on neonates and other groups possibly at risk (2015 update). LU: Publications Office, **2015**, https://doi.org/10.2772/45179.
[25] L. Larsson, P. Sandgren, S. Ohlsson, J. Derving, T. Friis-Christensen, F. Daggert, N. Frizi, S. Reichenberg, S. Chatellier, B. Diedrich, J. Antovic, S. Larsson, M. Uhlin, *Vox Sang.* **2021**, *116*, 60.
[26] G. Apte, J. Börke, H. Rothe, K. Liefeith, T. H. Nguyen, *ACS Appl. Bio Mater.* **2020**, *3*, 5574.
[27] Y. Liu, F. Zhang, S. Lang, L. Yang, S. Gao, D. Wu, G. Liu, Y. Wang, *Macromol. Biosci.* **2021**, *21*, 2100341.
[28] S. Yao, H. Y., S. Tian, R. Luo, Y. Zhao, J. Wang, *Smart Mater. Med.* **2024**, *5*, 166.
[29] X. H. Wu, Y. K. Liew, C. W. Mai, Y. Y. Then, *Int. J. Mol. Sci.* **2021**, *22*, 3341.
[30] T. Xiang, C.-D. L., R. Wang, Z.-Y. Han, S.-D. Sun, C.-S. Zhao, *J. Membr. Sci.* **2015**, *476*, 234.
[31] M. Ventre, C. F. Natale, C. Rianna, P. A. Netti, *J. R. Soc., Interface* **2014**, *11*, 25253035.
[32] L. B. Koh, I. Rodriguez, S. S. Venkatraman, *Biomaterials* **2010**, *31*, 1533.
[33] Y. Ding, Y. Leng, N. Huang, P. Yang, X. Lu, X. Ge, F. Ren, K. Wang, L. Lei, X. Guo, *J. Biomed. Mater. Res. – Part A* **2013**, *101 A*, 622.
[34] V. C. Bui, N. Medvedev, G. Apte, L. Y. Chen, C. Denker, A. Greinacher, T. H. Nguyen, *ACS Appl. Nano Mater.* **2020**, *3*, 6996.
[35] M. Emmert, F. Somorowsky, J. Ebert, D. Görick, A. Heyn, E. Rosenberger, M. Wahl, D. Heinrich, *Adv. Biol.* **2021**, *5*, 2000570.
[36] K. R. Milner, A. J. Snyder, C. A. Siedlecki, *J. Biomed. Mater. Res. – Part A* **2006**, *76*, 561.
[37] A. Kita, Y. Sakurai, D. R. Myers, R. Rounsevell, J. N. Huang, T. J. Seok, K. Yu, M. C. Wu, D. A. Fletcher, W. A. Lam, *PLoS One* **2011**, *6*, e26437.
[38] M. Hulander, A. Lundgren, L. Faxälv, T. L. Lindahl, A. Palmquist, M. Berglin, H. Elwing, *Colloids Surf., B* **2013**, *110*, 261.
[39] T. T. Pham, S. Wiedemeier, S. Maenz, G. Gastrock, U. Settmacher, K. D. Jandt, J. Zanow, C. Ludecke, J. Bossert, *Colloids Surf. B Biointerfaces* **2016**, *145*, 502.
[40] G. Apte, M. Hirtz, T.-H. Nguyen, *ACS Appl. Mater. Interfaces* **2022**, *14*, 24133.
[41] K. Stokes, K. Clark, D. Odetade, M. Hardy, P. Goldberg Oppenheimer, *Discov Nano* **2023**, *18*, 153.
[42] K. Y. Lee, D. J. Mooney, *Chem. Rev.* **2001**, *101*, 1869.
[43] B. V. Slaughter, S. S. Khurshid, O. Z. Fisher, A. Khademhosseini, N. A. Peppas, *Adv. Mater.* **2009**, *21*, 3307.
[44] M. A. Salati, J. Khazai, A. M. Tahmuri, A. Samadi, A. Taghizadeh, M. Taghizadeh, P. Zarrintaj, J. D. Ramsey, S. Habibzadeh, F. Seidi, M. R. Saeb, M. Mozafari, *Polymers (Basel)* **2020**, *12*, 1150.
[45] L. Wenger, C. P. Radtke, E. Gerisch, M. Kollmann, C. M. Niemeyer, K. S. Rabe, J. Hubbuch, *Front. Bioeng. Biotechnol.* **2022**, *10*, 928878.
[46] G. Apte, A. Lindenbauer, J. Schemberg, H. Rothe, T. H. Nguyen, *ACS Omega* **2021**, *6*, 10963.
[47] M. Ganjian, K. Modaresifar, D. Rompolas, L. E. Fratila-Apachitei, A. A. Zadpoor, *Acta Biomater.* **2022**, *140*, 717.
[48] C. J. van Oss, W. Zingg, O. S. Hum, A. W. Neumann, *Thromb. Res.* **1977**, *11*, 183.
[49] Z. Huang, H. Ghasemi, *Adv. Colloid Interface Sci.* **2020**, *284*, 102264.
[50] E. Arzt, H. Q., R. M. McMeeking, *Prog. Mater. Sci.* **2021**, *120*, 100823.
[51] R. Hensel, R. H., S. Aland, H.-G. Braun, A. Voigt, C. Neinhuis||, C. Werner, *Langmuir* **2013**, *29*, 1100.
[52] Y. Xue, P. L., H. Lin, H. Duan, *Appl. Mech. Rev.* **2016**, *68*, 030803.
[53] M. Nobili, J. Sheriff, U. Morbiducci, A. Redaelli, D. Bluestein, *ASAIO J.* **2008**, *54*, 64.
[54] W. A. Lam, O. Chaudhuri, A. Crow, K. D. Webster, T. D. Li, A. Kita, J. Huang, D. A. Fletcher, *Nat. Mater.* **2011**, *10*, 61.
[55] T. H. Nguyen, R. Palankar, V. C. Bui, N. Medvedev, A. Greinacher, M. Delcea, *Sci Rep.* **2016**, *6*, 25402.
[56] G. Apte, M. Hirtz, T. H. Nguyen, *ACS Appl. Mater. Interfaces* **2022**, *14*, 24133.
[57] P. Kantam, V. K. M., T. K. Jammu, R. M. Sabino, S. Vallabhuneni, Y. J. Kim, A. K. Kota, K. C. Popat, *Adv. Mater. Interfaces* **2024**, *11*, 2300564.
[58] L. Y. Chen, N. Khan, A. Lindenbauer, T. H. Nguyen, *Bioconjug. Chem.* **2022**, *33*, 1574.
[59] V. Hernández, D. Ibarra, J. F. Triana, B. Martínez-Soto, M. Faúndez, D. A. Vasco, L. Gordillo, F. Herrera, C. García-Herrera, A. Garmulewicz, *Materials* **2022**, *15*, 3954.
[60] A. Akhtar, V. Farzam Rad, A.-R. Moradi, M. Yar, M. Bazzar, *Smart Materials in Medicine* **2023**, *4*, 337.
[61] N. D. H. Grubhofer, Patent "Fixing agar for agarose gel to plastics foil - with precoating of foil with adhesive polymer layer contg. maleic anhydride Gps"(No. DE3032071A1) **1980**.
[62] H. Qanash, *Hail J. Health Sci.* **2021**, *3*, 1.
[63] M. Ferri, F. Chiellini, G. Pili, L. Grimaldi, E. T. Florio, S. Pili, F. Cucci, G. Latini, *Int. J. Pharm.* **2012**, *430*, 86.
[64] J. R. Stubbs, S. A. Tran, R. L. Emery, S. A. Hammel, A. L. Haugen, M. D. Zielinski, S. P. Zietlow, D. Jenkins, *Transfusion* **2017**, *57*, 2836.
[65] S. Bagel-Boithias, S.-M. Valeérie, D. Bourdeaux, V. Tramier, A. Boyer, J. Chopineau, *Am. J. Health-Syst. Pharm.* **2005**, *62*, 182.
[66] L. Bernard, T. Eljezi, H. Clauson, C. Lambert, Y. Bouattour, P. Chennell, B. Pereira, V. Sautou, *PLoS One* **2018**, *13*, 0192369.
[67] S. Kreve, A. C. D. Reis, *Jpn Dent. Sci. Rev.* **2021**, *57*, 85.
[68] N. Hadjesfandiari, P. Schubert, S. Fallah Toosi, Z. Chen, B. Culibrk, S. Ramirez-Arcos, D. V. Devine, D. E. Brooks, *Transfusion* **2016**, *56*, 2808.
[69] J. Schemberg, A. E. Abbassi, A. Lindenbauer, L.-Y. Chen, A. Grodrian, X. Nakos, G. Apte, N. Khan, A. Kraupner, T.-H. Nguyen, G. Gastrock, *ACS Appl. Mater. Interfaces* **2022**, *14*, 48011.
[70] V. Hernandez, D. Ibarra, J. F. Triana, B. Martinez-Soto, M. Faundez, D. A. Vasco, L. Gordillo, F. Herrera, C. Garcia-Herrera, A. Garmulewicz, *Mater.* **2022**, *15*, https://doi.org/10.3390/ma15113954.